Two-dimensional analysis of the interface state effect on current gain for a 4H–SiC bipolar junction transistor

Zhang You-Run(张有润)†, Zhang Bo(张 波), Li Zhao-Ji(李肇基), and Deng Xiao-Chuan(邓小川)

State Key Laboratory of Electronic Thin Films and Integrated Devices, University of Electronic Science and Technology of China, Chengdu 610054, *China*

(Received 18 September 2009; revised manuscript received 15 November 2009)

This paper studies two-dimensional analysis of the surface state effect on current gain for a 4H–SiC bipolar junction transistor (BJT). Simulation results indicate the mechanism of current gain degradation, which is surface Fermi level pinning leading to a strong downward bending of the energy bands to form the channel of surface electron recombination current. The experimental results are well-matched with the simulation, which is modeled by exponential distributions of the interface state density replacing the single interface state trap. Furthermore, the simulation reveals that the oxide quality of the base emitter junction interface is very important for 4H–SiC BJT performance.

Keywords: 4H–SiC, bipolar junction transistor, current gain, interface state trap

PACC: 7155, 7340, 7280

1. Introduction

Silicon carbide (SiC) is a very attractive material for high-voltage, high-temperature and high-power applications due to its wide bandgap, high breakdown field, and high thermal conductivity. The 4H–SiC bipolar junction transistor (BJT) is a promising switching device and considerable progress has been made in recent years.[1−4] It is an intrinsically normally-off device, does not have gate oxide problems, and conducts high current with a low forward voltage. One major challenge for the commercialization of SiC power BJTs is performance degradation in current gain due to the high density of surface states along the SiC/SiO_2 interface on the etched sidewalls at the emitter–base perimeter.[5] The origin of the interface traps is still unclear but recent calculations suggest that silicon interstitials or carbon dimers are possible origins.[6] Therefore, the development of an improved silicon oxide layer is a key issue for achieving high current gain SiC BJTs. To date, some methods have been proposed in SiC metal-oxide semiconductor field-effect transistor (MOSFET) technology to reduce the interface trap density at the SiO_2/SiC interface. A promising method is the oxidation or postoxidation annealing treatment in an ambient containing nitric oxide (NO) or nitrous oxide (NO_2) gases.[7]

In this paper, two-dimensional analysis of the interface trap effects on the extrinsic base of 4H–SiC BJT is investigated. The influence of interface trap on current gain is discussed. It is considered that the interface states are characterized by a continuous state distribution with an exponential function in the bandgap replacing the single trap at a given energy level. The simulation results indicate that surface Fermi level pinning on the extrinsic p-base region leads to surface depletion and a strong downward bending of the energy bands to form the channel of surface electron recombination current, which is the main component of base current. This mechanism is a very important cause of the current gain degradation. Furthermore, the I–V characteristic curves modeled by the continuous interface state distributions are perfectly matched with the experimental results.

2. Device structure and physical models

The simplified cross-section of a 4H–SiC BJT is shown in Fig. 1. The thickness of the collector drift-region is 15 μm with a uniform doping of 4.8×10^{15} cm^{-3} and the thickness p-base is taken as 1 μm with a uniform doping of 2×10^{17} cm^{-3}, while the emitter doping is 3×10^{19} cm^{-3} with thickness of 1.5 μm. The guard rings doping is taken as 5×10^{17} cm^{-3}. The width of the emitter and implanted base fingers are 10 μm and 5 μm and a temperature

†Corresponding author. E-mail: yrzhang@uestc.edu.cn

© 2010 Chinese Physical Society and IOP Publishing Ltd

of 300 K is employed as the default in the simulations.

The surface states are assumed to exist on each exposed surface between the emitter–base regions (shaded regions in Fig. 1). Acceptor-type traps have been evaluated in this work.[8,9] The location of trap levels (E_t) is expressed by the distance from the conduction band bottom E_C, as $E_C - E_t$. During different technological processes, deep levels and trap centres with different concentrations and energy distributions can be formed in crystals.

The 4H–SiC BJT characteristics are simulated by the simulator ATLAS. The different physical models used simultaneously are SRH (Shockley–Read–Hall) and Auger for generation and recombination, BGN for bandgap narrowing, Caughey–Thomas model for mobility and finally, Incomplete for incomplete ionization of dopants. Traps are included in the simulator by the use of SRH statistics. The charged trap density is added to the Poisson equation, and a generation recombination term due to the traps is included in the continuity equations.[10,11]

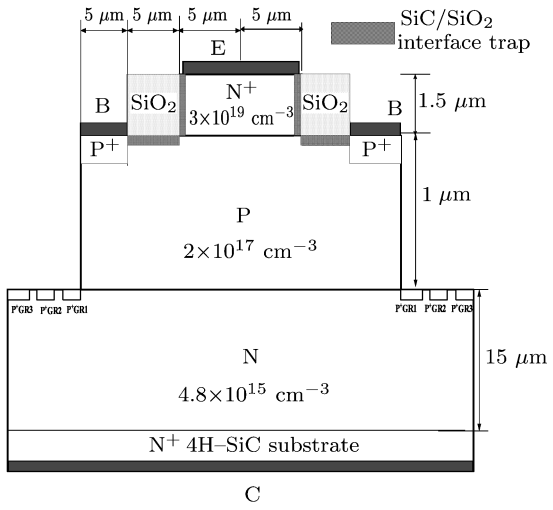


Fig. 1. 4H–SiC BJT structure for analysis.

2.1. Bandgap narrowing model

A high concentration of free carriers in a semiconductor can cause a significant reduction in bandgap. At high doping levels, carrier–carrier interaction, carrier–impurity interaction and overlap of the electron wave functions are not negligible. These bandgap narrowing effects are taken into account in band edge displacements which can be described as[12]

$$\begin{aligned}\Delta E_C &= (-1.5\times10^{-2})\left(\frac{N_D^+}{10^{18}}\right)^{1/3} \\ &\quad + (-2.93\times10^{-3})\left(\frac{N_D^+}{10^{18}}\right)^{1/2}, \\ \Delta E_V &= (1.9\times10^{-2})\left(\frac{N_D^+}{10^{18}}\right)^{1/4} \\ &\quad + (8.74\times10^{-3})\left(\frac{N_D^+}{10^{18}}\right)^{1/2}. \end{aligned} \quad (1)$$

Bandgap narrowing has an important effect in bipolar transistors by increasing the minority carrier concentration in the emitter, thus reducing its efficiency.

2.2. Mobility models

The Caughey–Thomas model[13] is commonly used for describing the carrier mobility of SiC. The mobilities of electrons and holes at low electric fields are both dependent on the doping level and temperature, and they are given respectively by

$$\begin{aligned}\mu_n(\mathrm{cm}^2/V_s) &= \frac{947\times(T/300)^{-2}}{1+[N_i/(1.94\times10^{17})]^{0.61}}, \\ \mu_p(\mathrm{cm}^2/V_s) &= 15.9+\frac{124\times(T/300)^{-2}}{1+[N_i/(1.76\times10^{19})]^{0.34}}, \end{aligned} \quad (2)$$

where N_i denotes the total concentration of ionized impurities.

At high electric fields, the carrier drift velocity saturates due to an increase in optical phonon scattering and reaches the saturation velocity. The mobilities of electrons and holes at high electric fields can be expressed respectively as:

$$\begin{aligned}\mu_n(\mathrm{cm}^2/V_s) &= \frac{\mu_{n0}}{\left[1+\left[\frac{\mu_{n0}E}{V_{sat}}\right]^2\right]^{0.5}}, \\ \mu_p(\mathrm{cm}^2/V_s) &= \frac{\mu_{p0}}{1+\left[\frac{\mu_{n0}E}{V_{sat}}\right]}, \end{aligned} \quad (3)$$

where μ_{n0} and μ_{p0} are the mobilities of electrons and holes at low electric fields respectively. V_{sat} is the saturation velocity with a value of 2×10^7 cm·s^{-1} for 4H–SiC.

2.3. Carrier lifetime model

The SRH lifetime depends on the doping concentration and the temperature. The doping dependence of the SRH lifetime is modeled with the Scharfetter

relation,[13] and the temperature dependence is modeled by a power law.[13] Thus, the electron lifetime is expressed as follows:

$$\tau_{\rm n} = \frac{\tau_{{\rm max},n}\left(\dfrac{T}{300}\right)^{1.72}}{1+\left(\dfrac{N_{\rm i}}{3\times 10^{17}}\right)^{0.3}}, \tag{4}$$

where T is the lattice temperature in K, $N_{\rm i}$ is the total concentration of ionized impurities, and $\tau_{{\rm max},n}$ is the electron lifetime in the material without impurities at 300 K. The parameter α is cited from Ref. [14] and the parameter γ is taken from Ref. [15]. The relation $\tau_{\rm n} = 5\tau_{\rm p}$ is used in the simulation.

2.4. Incomplete ionization model

The donor and the acceptor energy levels ($E_{\rm D}$ and $E_{\rm A}$) in SiC are deeper than the thermal energy at room temperature, so the dopants in SiC are not fully ionized even above room temperature.[16] The ionized concentration for donors ($N_{\rm D}^{+}$) and acceptors ($N_{\rm A}^{+}$) are given by

$$N_{\rm D}^{+} = \frac{N_{\rm D}}{1+g_{\rm c}\exp\left[\dfrac{E_{\rm Fn}-E_{\rm D}}{kT}\right]},$$
$$N_{\rm A}^{+} = \frac{N_{\rm A}}{1+g_{\rm v}\exp\left[\dfrac{E_{\rm Fp}-E_{\rm A}}{kT}\right]}, \tag{5}$$

where $N_{\rm D}$ and $N_{\rm A}$ are donor and acceptor impurities of concentration added to the semiconductor crystal, $E_{\rm Fn}$ and $E_{\rm Fp}$ are the quasi-Fermi levels of electrons and holes, respectively. Due to the lack of specific information for SiC, the donor energy level degeneracy factor $g_{\rm c}$ and acceptor energy level degeneracy factor $g_{\rm v}$ are usually assumed to have the same values as those in Si. For energy levels of nitrogen donor in 4H–SiC, a dopant ionization energy $E_{\rm Fn} - E_{\rm D} = 42$ meV and $g_{\rm c} = 2$ can be used. The p-type doping can be achieved with Al acceptors with ionization energy $E_{\rm Fp} - E_{\rm A} = 191$ meV and $g_{\rm v} = 4$.

2.5. The SRH recombination

The carrier recombination model is the SRH equation. The SRH recombination rate can be defined as

$$R_{\rm SRH} = \frac{np - n_{\rm i}}{\tau_{\rm p}\left[n + n_{\rm i}\exp\left(\dfrac{E_{\rm t}-E_{\rm i}}{kT}\right)\right] + \tau_{\rm n}\left[p + n_{\rm i}\exp\left(-\dfrac{E_{\rm t}-E_{\rm i}}{kT}\right)\right]}, \tag{6}$$

where $R_{\rm SRH}$ is SRH recombination rate, n and p are electron and hole densities, respectively, $n_{\rm i}$ is the intrinsic carrier density, $E_{\rm t}$ is the energy level of the recombination centres, $\tau_{\rm n}$ and $\tau_{\rm p}$ are electron and hole lifetimes, respectively, which are dependent on the doping level and the temperature.

3. Results and discussion

The interface trap density of states inside the 4H–SiC semiconductor bandgap is modeled as consisting of two components: one is the density of trap states in the middle of the bandgap that has a constant density with energy; the other is the density of trap states as the tail of a distribution near the conduction band edges; the maximum lies in the conduction band. These band-tail states are very large in number and give rise to a huge population of occupied traps at the interface.[17,18]

For acceptor-type traps, the density of states can be written as follows:

$$D_{\rm it}(x,y,E_{\rm t}) = D_{\text{it-mid}} + D_{\text{it-edge}} \times \exp\left(\frac{E_{\rm t}-E_{\rm C}}{\varsigma}\right), \tag{7}$$

where $E_{\rm t}$ is the energy level inside the bandgap, $E_{\rm C}$ is the conduction band energy, $D_{\text{it-mid}}$ is the midgap interface trap density of states, $D_{\text{it-edge}}$ is the band–edge interface trap density of states, and ζ is the characteristic energy for the exponential portion of the trap density of state. Values for $D_{\text{it-mid}}$, $D_{\text{it-edge}}$ and ζ are obtained throughout the experiment. The density of occupied acceptor type interface state traps is

$$N_{\rm it} = \int_{E_{\rm midgap}}^{E_{\rm C}} D_{\rm it}(E) f_{\rm n}(E) {\rm d}E. \quad (8)$$

Here, $f_{\rm n}(E)$ is the Fermi distribution function:

$$f_{\rm n}(E,x) = \frac{1}{1+\frac{1}{2}\frac{N_{\rm C}}{n(x)}\exp\left(\frac{E-E_{\rm C}}{kT}\right)}, \quad (9)$$

where $N_{\rm C}$ is the conduction band density of states, $n(x)$ is the density of electrons on the surface, $E_{\rm C}$ is the conduction band minimum, and $E_{\rm midgap}$ is the midgap point.

Experimental studies reveal that the density of interface states in SiC/SiO_2, which is determined by constant-capacitance deep level transient spectroscopy,[19] is of the order of 10^{11}–10^{13} $cm^{-2}\cdot eV^{-1}$ and increases from approximately midgap towards conduction band edge. The capture cross-section of traps in SiC can be changed in the range 10^{-16} to 10^{-21} cm^2.[20] The trap density of state profile extracted from experimental data is shown in Fig. 2.

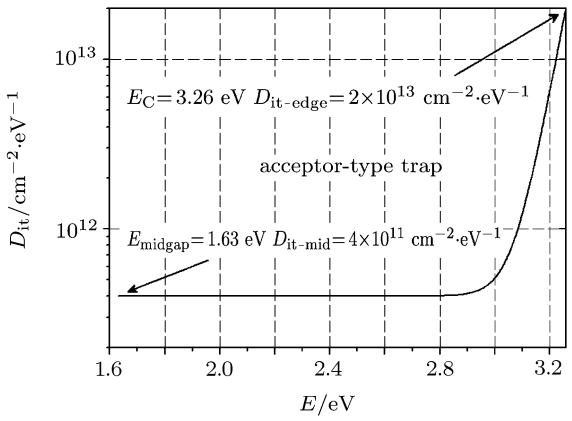


Fig. 2. Acceptor-type trap density of states function to be modeled. The values for the midgap $D_{\rm it\text{-}mid}$, and the band-edge $D_{\rm it\text{-}edge}$, densities of states and the band-tail energy for the exponential portion of the trap density of state ζ are 4×10^{11} $cm^{-2}\cdot eV^{-1}$, 2×10^{13} $cm^{-2}\cdot eV^{-1}$ and 67 meV, respectively. The energy band scale is shown from the middle of the bandgap to the minimum of the conduction band for 4H–SiC. The valence band is at 0 eV.

By matching with the real experimental data of 4H–SiC I–V characteristic curves, the trap of state density is 4×10^{11} $cm^{-2}\cdot eV^{-1}$ in the midgap and an exponential rise to 2×10^{13} $cm^{-2}\cdot eV^{-1}$ within the conduction band edges 0.5 eV is assumed. In our simulation, an exponential distribution of the interface state is employed to replace the single interface state energy level. To compare with the exponential interface state distribution, a constant state density of traps $D_{\rm it} = 2\times10^{13}$ $cm^{-2}\cdot eV^{-1}$ at the single interface state energy level from 0.1 eV to 0.5 eV is applied. A capture cross-section of $\delta = 6\times10^{-15}$ cm^{-2} and a degeneracy factor of 1.0 are used.

To better understand the surface recombination behaviour, we study the carriers that reach the surface and recombine. Figure 3 plots the electron current stream lines showing that the pattern of carriers flowing to the surface to recombine in the extrinsic base. Note that the flow of electrons along the extrinsic base surface is strongly channeled with the large surface recombination velocity leading to a substantial surface recombination current. This surface electron channel is caused by Fermi-level pinning that leads to the formation of saddle point at the surface through which electrons are injected.

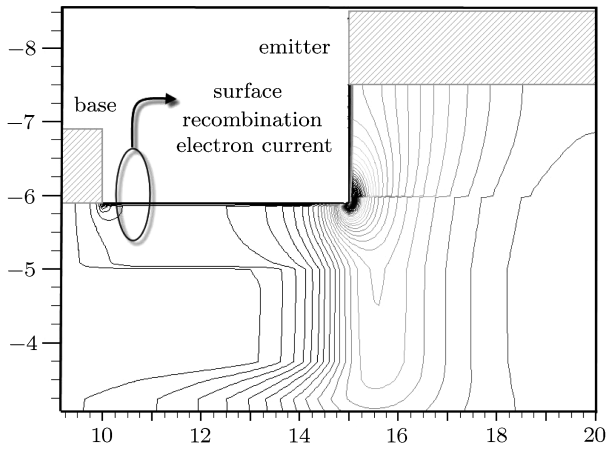


Fig. 3. Current stream lines showing how carriers reach the surface of the extrinsic base. Surface recombination occurs along the exposed surface of the extrinsic base, which stretches between 10 μm and 15 μm laterally. Collector contacts are outside the range of the figure.

Conduction and valence band diagrams across the base extrinsic cut under the forward bias are shown in Fig. 4. It is seen that surface Fermi level pinning on the extrinsic p-base region leads to surface depletion and a strong downward bending of the bands. The amount of band bending is of the order of the base material hole Schottky barrier height for the exposed surface. Moreover, the band energy levels are bent downwards with different interface state levels ($E_{\rm t}$). From $E_{\rm C} - E_{\rm t} = 0.1$ eV to 0.5 eV, the extrinsic base surface shows a much stronger downward band bending comparing with the continuous interface state energy level. It can be explained that this bending induces the saddle potential at the emitter periphery to inject electrons onto the extrinsic base

surface where they recombine at the surface according to SRH statistics.[21,22]

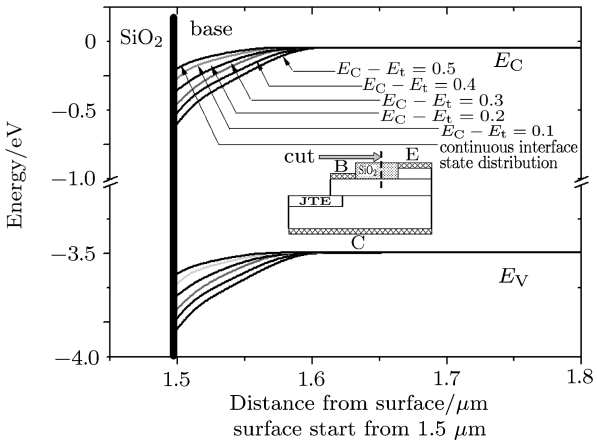


Fig. 4. Fermi level pinning of energy bandgap with different interface state trap level distribution.

Figure 5 shows the DC common current gain ($\beta = I_C/I_B$) versus collector current with an active area of 3×3 mm^2 at room temperature. The carrier lifetime of $\tau_n = 30$ ns, $\tau_p = 6$ ns and a capture cross section of $\delta = 6 \times 10^{-15}$ cm^2 with the acceptor-type interface traps is used and the interface trap density $D_{it} = 2 \times 10^{13}$ cm^{-2}·eV^{-1} is also applied in the simulations of the single interface level. It should be noted that the simulated results of the continuous interface state distribution of the exponential function are in good agreement with the experimental data in Fig. 6, which depicts the collector current–voltage (I_C–V_{CE}) characteristics under the base current bias (I_B) varied from 200 mA to 800 mA in a step of 200 mA.[1] We mainly compare the continuous interface state distribution with the single interface state level. It can be seen that the DC current gain decreases with the depth of single interface trap energy level away from the conduction band ($E_C - E_t$) and gradually saturates as $E_C - E_t > 0.3$ eV. The effect of current gain is due to the different degree of interface state pinning. As the pinning gradually increases ($E_C - E_t$ from 0.1 eV to 0.5 eV), many more electrons inject from the intrinsic base into the extrinsic base surface to cause a greater base surface recombination current, which is the main component of the base current. So the common DC current gain considering surface recombination can be expressed as

$$\beta^{-1} = \beta_{rB}^{-1} + \beta_{rSCR}^{-1} + \beta_E^{-1} + \beta_{rSurf}^{-1}, \qquad (10)$$

where β_{rB}^{-1} is the factor of the recombination in neutral bulk of the base, β_{rSCR}^{-1} is the factor of the recombination in the emitter–base space charge region, β_E^{-1} is the factor related to the emitter injection efficiency, and β_{rSurf}^{-1} is the new factor of the recombination on the extrinsic base surface. When $E_C - E_t$ is 0.3 eV∼0.5 eV, interface state trap level is pinned to the electron quasi-Fermi level of the surface leading to the maximum surface recombination rate. So current gain decreases and gradually saturates due to the base surface recombination current approaching the maximum.

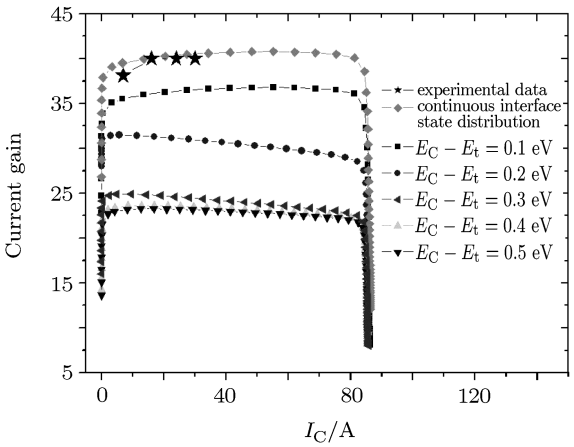


Fig. 5. The DC common current gain versus collector current with an active area of 3×3 mm^2. Simulations and comparison to experiment indicate the good match based on the continuous interface state distribution.

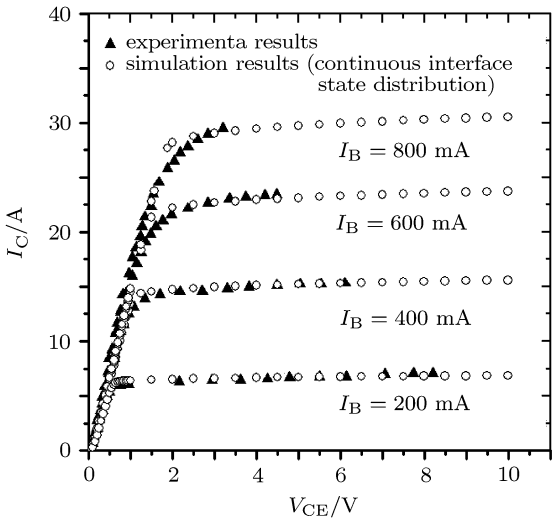


Fig. 6. The 4H–SiC BJT I–V curves are compared with the experimental results and simulation results applied the continuous distribution interface state distribution. Base current is varied from 200 mA to 800 mA.

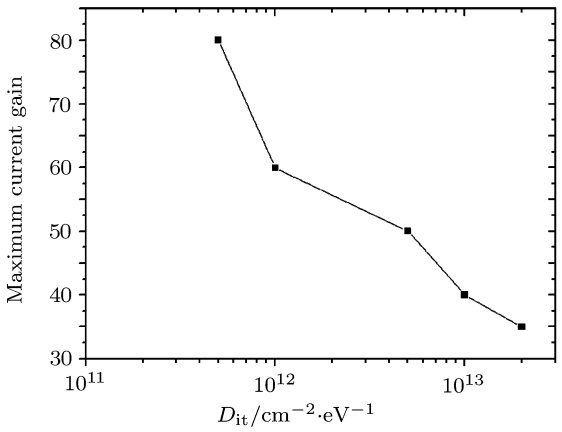


Fig. 7. Maximum current gain versus the interface state density at the SiC/SiO_2 interface with the interface state energy level of $E_C - E_t = 0.1$ eV.

The ability to influence the maximum current gain in device simulations of BJTs by varying $D_{\rm it}$ from 5×10^{11} $\rm cm^{-2}\cdot eV^{-1}$ to 2×10^{13} $\rm cm^{-2}\cdot eV^{-1}$ is illustrated in Fig. 7. The interface state energy level is assumed at $E_C - E_t = 0.1$ eV. A decreasing current gain is observed as $D_{\rm it}$ increases owing to more surface recombination. It can be seen that the oxide quality of the base–emitter junction interface is very important. Nowadays, the reactive ion etching process step will definitely introduce some defects at the base–emitter junction and at the surface, which could cause severe problems of degradation. Therefore, the more mature SiC/SiO_2 interface process needs to be investigated.

4. Conclusions

A two-dimensional analysis of surface recombination on current gain for a 4H–SiC BJT is studied. The mechanism of current gain degradation is indicated by the simulation results, which are well-matched with the data extracted from the experiment. The good simulation is based on the model of the continuous interface state distributions replacing the single interface state trap.

References

[1] Krishnaswami S, Agarwal A, Ryu S H, Capell C, Richmond J, Palmour J, Balachandran S, Chow T P, Bayne S, Geil B, Jones K and Scozzie C 2005 *Electron Device Lett.* **26** 175

[2] Balachandran S, Chow T P, Agarwal A, Scozzie C and Jones K A 2005 *Electron Device Lett.* **26** 470

[3] Ivanov P A, Levinshtein M E, Agarwal A K, Krishnaswami S and Palmour J W 2006 *Electron Devices* **53** 1245

[4] Zhang J H, Li X Q, Alexandrov P, Fursin L, Wang X H and Zhao J H 2008 *Electron Devices* **55** 1899

[5] Gao Y, Huang A Q, Zhang Q C, Krishnaswami S and Agarwal A K 2007 *Proc. 19th Int. Symp. Power Semiconductor Devices Ics* 121

[6] Knaup J M, Frauenheim P D T, Gali A, Hajnal Z and Choyke W J 2005 *Phys. Rev.* B **72** 115323

[7] Soares G V, Baumvol I J R, Hold L, Kong F, Dimitrijev J H S, Radtke C and Stedile F C 2007 *Appl. Phys. Lett.* **91** 041906

[8] Powell S K, Goldsman N, McGarrity J M, Bernstein J, Scozzie C J and Lelis A 2002 *J. Appl. Phys.* **92** 4053

[9] Potbhare S, Goldsman N, Lelis A, McGarrity J M, McLean F B and Habersat D 2008 *Electron Devices* **55** 2029

[10] Zhang Y R, Zhang B, Li Z J, Deng X C and Liu X L 2009 *Chin. Phys.* B **18** 3995

[11] Deng X C, Feng Z, Zhang B, Li Z J, Li L and Pan H S 2009 *Chin. Phys.* B **18** 3018

[12] Lindefelt U 1998 *J. Appl. Phys.* **84** 2628

[13] Device Simulator Atlas 2008 *Atlas User's Manual* Silvaco International

[14] Kordina O and Bergman J P 1996 *Appl. Phys. Lett.* **69** 679

[15] Ruff M, Mitlehner H and Helbig R 1994 *Electron Devices* **41** 1040

[16] Capano M A, Santhakumar R, Venugopal R, Melloch M R and Cooper J A 2000 *J. Electr. Mater.* **29** 210

[17] Vathulya V R and White M H 2000 *Electron Devices* **47** 2018

[18] Saks N S, Mani S S and Agarwal A K 2000 *Appl. Phys. Lett.* **76** 2250

[19] Yano H, Katafuchi F and Matsunami H 1999 *Electron Devices* **46** 504

[20] Constand A, Camara N, Godignon P and Camassel J 2009 *Appl. Phys. Lett.* **94** 063508

[21] Tao N G M, Liu H G and Bolognesi C R 2005 *Electron Devices* **52** 1061

[22] Tiwari S and David J F 1989 *Electron Devices* **36** 2105